Biointerphases
a SpringerOpen Journal

ORIGINAL ARTICLE Open Access

Evaluating protocols and analytical methods for peptide adsorption experiments

Kenan P Fears[1], Dmitri Y Petrovykh[1,2,3*] and Thomas D Clark[1*]

Abstract

This paper evaluates analytical techniques that are relevant for performing reliable quantitative analysis of peptide adsorption on surfaces. Two salient problems are addressed: determining the solution concentrations of model GG–X–GG, X_5, and X_{10} oligopeptides (G = glycine, X = a natural amino acid), and quantitative analysis of these peptides following adsorption on surfaces. To establish a uniform methodology for measuring peptide concentrations in water across the entire GG–X–GG and X_n series, three methods were assessed: UV spectroscopy of peptides having a C-terminal tyrosine, the bicinchoninic acid (BCA) protein assay, and amino acid (AA) analysis. Due to shortcomings or caveats associated with each of the different methods, none were effective at measuring concentrations across the entire range of representative model peptides. In general, reliable measurements were within 30% of the nominal concentration based on the weight of as-received lyophilized peptide. In quantitative analysis of model peptides adsorbed on surfaces, X-ray photoelectron spectroscopy (XPS) data for a series of lysine-based peptides (GGKGG, K_5, and K_{10}) on Au substrates, and for controls incubated in buffer in the absence of peptides, suggested a significant presence of aliphatic carbon species. Detailed analysis indicated that this carbonaceous contamination adsorbed from the atmosphere after the peptide deposition. The inferred adventitious nature of the observed aliphatic carbon was supported by control experiments in which substrates were sputter-cleaned by Ar^+ ions under ultra-high vacuum (UHV) then re-exposed to ambient air. In contrast to carbon contamination, no adventitious nitrogen species were detected on the controls; therefore, the relative surface densities of irreversibly-adsorbed peptides were calculated by normalizing the N/Au ratios by the average number of nitrogen atoms per residue.

Background

The interactions between biomolecules and surfaces play a crucial role in many technological processes and devices, such as molecular separation, biofouling, biosensors, biomedical implants, and biomimetic materials [1-6]. To begin understanding the processes by which proteins adsorb to surfaces, small peptides have been used as model systems because they avoid many challenges associated with the complexity inherent in natural proteins [7-10]. In particular, model peptides can be designed to isolate molecular interactions involving an individual amino acid residue, a peptide sequence, or a structural subunit of interest [11-15].

An example of a system designed to investigate surface interactions of an individual amino acid residue are the model oligopeptides examined in this work: they are representative of (or related to) the general GG–X–GG and X_n ($n = 5$ or 10) series, where G is glycine and X is one of the naturally occurring amino acids. The diversity of physicochemical properties of peptides across such a series produces several important analytical considerations that must be carefully addressed before a meaningful quantitative comparison of peptide adsorption on surfaces can be carried out.

Solution analysis

We first considered issues that are particularly easy to overlook while planning a systematic survey of peptide-surface interactions: the peptides in a model series should have similar solubility in a common solvent and should be stable in that solvent against aggregation. A related consideration in systematic quantitative measurements is

* Correspondence: dmitri.petrovykh@inl.int; thomas.clark@nrl.navy.mil
[1]Division of Chemistry, Naval Research Laboratory, Washington, DC 20375-5342, USA
[2]Department of Physics, University of Maryland, College Park, MD 20742, USA
Full list of author information is available at the end of the article

reliably establishing the concentration of different peptides across the entire model series, as methods for determining peptide concentration can depend on the size, structure, and residue composition of the peptides. Therefore, for our model peptides, we calculated concentration values from dry weight of dissolved peptides, which is by far the most commonly used method for calculating peptide concentrations, and systematically evaluated the performance of three common techniques for measuring peptide concentrations: (1) UV spectroscopy of peptides having a C-terminal tyrosine [16,17], (2) the bicinchoninic acid (BCA) protein assay [17-19], and (3) amino acid (AA) analysis [20].

Incorporating tyrosine, tryptophan, or cysteine residues, which exhibit absorbance bands at 280 nm, can be used to determine the peptide concentration based on the assumption that a molecule's extinction coefficient is a linear combination of its chromophores' coefficients [21]. More generally, UV spectroscopy provides relative concentrations of proteins or peptides based on a strong absorbance band at 195 nm; however, that band can contain contributions from both the peptide backbone and certain side chains, most notably aromatic side chains [17,22]. Thus, the extinction coefficient at 195 nm must be independently verified and calibrated for each peptide sequence.

The BCA protein assay [17-19], which relies on the chelation and subsequent reduction of Cu^{2+} ions by the amide backbone of polypeptide chains, has been used extensively to quantify proteins in solution, whereby the unknown protein concentration is calculated based on comparison to a calibration curve for a standard solution of bovine serum albumin (BSA). The BCA assay has been reported as both successful [12,23,24] and potentially problematic [19] for peptide sequences similar to ours, thus requiring us to evaluate the effectiveness of BCA measurements for GG–X–GG and X_n model peptides.

For selected model peptides, we examined the applicability of AA analysis [20], which relies on acid hydrolysis to cleave the peptide bonds and yield the individual amino acids; however, cysteine and tryptophan side chains degrade during acid hydrolysis, limiting the generality of this method.

Surface analysis

Having established reliable protocols for preparing and characterizing peptide solutions, our next task is to characterize the adsorption of peptides on surfaces. Fluorescent [25,26] and radioactive [27,28] labels have been used to quantify surface-adsorbed peptides. However, the hazards and costs preclude radiolabeling in broad surveys like ours, while fluorescence quenching renders fluorescent labels impractical for quantitative analysis on important model surfaces, such as gold and other coinage metals. Label-free techniques, such as ellipsometry, surface plasmon resonance (SPR) spectroscopy, and quartz crystal microbalance (QCM) measurements, can quantify adsorbates on a surface [28-31]. Unfortunately, these techniques cannot distinguish between adsorbed peptides and, for example, adventitious contaminants. The effect of adventitious hydrocarbons on the adsorption of *small* peptides has not been carefully examined, but displacement or masking clearly cannot be assumed *a priori*, as is done for high-molecular-weight proteins. In principle, depositing and measuring peptides *in situ* can eliminate hydrocarbon adsorption. Rigorously cleaning the surfaces *in situ* before peptide deposition, however, is not trivial and may merely replace hydrocarbons by other surfactants.

UV spectroscopy has been used as a label-free technique to quantify protein adsorption [32,33]; however, the selection of suitably transparent substrates for UV spectroscopy is limited. X-ray photoelectron spectroscopy (XPS) and time-of-flight secondary ion mass spectrometry (ToF-SIMS) are label-free surface analysis techniques that have been increasingly used for analysis of biomolecules irreversibly adsorbed on surfaces [27,34,35]. Neither technique suffers from the substrate limitations of UV spectroscopy; XPS particularly excels at quantifying adsorbates because it relies on ratios of adsorbate to substrate signals [36] rather than on reference adsorbate peaks, which can be affected by matrix effects and surface contaminants in ToF-SIMS measurements.

We addressed analytical considerations outlined above for both solution and surface characterization of model peptides. We examined protocols for determining the solution concentrations of model peptides before surface adsorption, then proceeded to establish protocols for the quantification of model peptides after surface adsorption on inorganic substrates using XPS. Our overall objective was to develop and validate a set of practical methods and protocols that would be generally applicable to surface analysis of model peptides and similarly biofunctionalized surfaces.

Methods

Concentration measurements

The peptides used in this study were synthesized and purified (>98%) by GenScript USA Inc. We chose to have the N- and C-termini of the peptides acetylated ($–COCH_3$) and amidated ($–NH_2$) to eliminate possible effects of free amino and carboxylic acid groups, respectively, on the conformation [37], and, potentially, adsorption behavior of the peptides. All buffer reagents were used as received from Sigma-Aldrich Co. Stock solutions of the peptides were prepared using a 10 mM phosphate buffer, adjusted to a pH of 7.0 by mixing the appropriate amounts of NaH_2PO_4 and Na_2HPO_4 solutions. The nominal peptide

concentration based on the dry weight of lyophilized peptide added to buffer was recorded for comparison with other concentration measurement techniques.

Bicinchoninic acid assay

We measured the concentrations of the peptide stock solutions using a Pierce® BCA protein assay kit (Thermo Scientific) in accordance with the standard protocol. Peptides containing cysteine, tryptophan, or tyrosine residues were excluded from this analysis because these residues interfere with BCA assay [19]. Samples were prepared in aqueous solutions then mixed at a ratio of 1:8 with the working reagent in a 96-well plate and incubated at 37°C for 30 minutes. The well plates were allowed to cool to room temperature before measurements at 562 nm on a Safire multi-detection monochromator-based plate reader (Tecan). A calibration curve for the assay was constructed using serial dilutions (0–2,000 μg/mL) of a BSA standard.

UV absorbance

The concentrations of aqueous solutions of GGWGG and GGYGG were determined by measuring the absorbance peak at 280 nm. Additionally, we obtained a group of GG–X–GG and X_5 peptides labeled with a C-terminal tyrosine (*i.e.*, GG–X–GGY). We collected absorbance spectra on a Jasco J-815 spectrometer using a 1.0 mm path quartz cuvette held at 20°C by a Peltier temperature controller (Jasco). Molar concentrations were calculated according to Beer's Law:

$$A_{280nm} = \varepsilon_i \times L \times C \tag{1}$$

where ε_i is the molar extinction coefficient at 280 nm (M^{-1} cm^{-1}), L is the optical path length (cm), and C is the peptide concentration (M). This calculation is based on the assumption that only tyrosine or tryptophan side chains contribute to the absorbance peak at 280 nm. Therefore, the molar extinction coefficient of a peptide that contains a single tyrosine or tryptophan residue is 1280 M^{-1} cm^{-1} or 5690 M^{-1} cm^{-1}, respectively [21].

Amino acid analysis

AA analysis was performed by the Protein Chemistry Laboratory at Texas A&M University according to the following protocol. Aliquots of each peptide stock solution, except sequences containing cysteine or tryptophan, and the BSA control were mixed with two internal standards, norvaline and sarcosine, pipetted into borosilicate glass culture tubes in triplicate and dried under vacuum to yield approximately 20 μg of BSA or 10 μg of peptide in each tube. The samples were then subjected to acid hydrolysis by 6 N aqueous HCl at 150°C for 1.5 hours under argon and in the presence of phenol to limit halogenation of tyrosine residues. The hydrolyzed samples were resuspended in a 0.4 N borate buffer (pH 10) and transferred into an AminoQuant autosampler for automated derivatization by *o*-phthalaldehyde (OPA) and 9-fluoromethyl-chloroformate (FMOC). Following derivatization, the residues were separated by reversed-phase HPLC, and detected and quantitated by UV absorbance or fluorometry.

Circular dichroism

We used CD spectroscopy to assess the secondary structure of the peptides in solution. UV absorbance and CD spectra were simultaneously collected using a Jasco J-815 spectrometer over the wavelength range of 185–290 nm in a 1.0-mm path length quartz cuvette. Scans were acquired at a rate of 20 nm/min; each spectrum represents the accumulation of five scans. The temperature of the cuvette was maintained at 20°C throughout analysis to minimize solvent evaporation and temperature fluctuations. We baseline-corrected all CD and absorbance spectra of the peptide solutions by subtracting the corresponding pure buffer spectrum. Baseline-corrected CD spectra were converted from raw ellipticity (θ, mdeg) to molar ellipticity ($[\theta]$, deg × cm^2/dmol) using the following equation:

$$[\theta] = \frac{\theta \times MW}{10{,}000 \times C \times L \times N} \tag{2}$$

where MW is the molecular weight of the peptide (g/mol), C is the peptide concentration (g/mL), L is the optical path length through buffer (cm), and N is the number of AA residues.

Surface analysis

Substrate preparation

We used the following substrates for peptide adsorption experiments: [100] silicon wafers (University Wafers), gold-coated (100 nm of Au over 5 nm of Ti) silicon wafers (Platypus Technologies), fused-quartz plates (Chemglass), and 10-mm diameter calcium fluoride windows (ISP Optics). The wafers and plates were cut into smaller pieces (ca. 1.0 cm^2) prior to the cleaning process. The CaF_2 windows were cleaned by sonicating them for 5 minutes in an aqueous 0.005% (v/v) Triton® X-100 solution followed by 98 wt.% H_2SO_4. We sonicated all other substrates for 5 min in the following sequence of solutions: 0.005% (v/v) Triton® X-100, "piranha" wash (7:3 H_2SO_4 (98 wt.%)/H_2O_2 (30 wt.%)), and RCA standard clean 1 (1:1:5 NH_4OH (28.0–30.0% NH_3 basis)/H_2O_2 (30 wt.%)/H_2O). (*Caution: piranha solution is extremely oxidizing, reacts violently with organics, and should only be stored in loosely tightened containers to avoid pressure buildup*). The substrates were thoroughly rinsed with 18 MΩ-cm deionized (DI) water after each sonication step

and blown dry with nitrogen gas at the completion of the cleaning process. All substrates were cleaned immediately before the adsorption experiments to limit their exposure to contaminants in the atmosphere.

X-ray photoelectron spectroscopy

We assessed the purity of peptide stock solutions by pipetting 3 μL drops onto warmed (ca. 75°C) Au substrates to form thick peptide films. XPS data were acquired at room temperature in an ultra-high vacuum analysis chamber with the base pressure $<5 \times 10^{-9}$ mbar using a commercial XPS instrument equipped with a monochromated Al Kα X-ray source. These reference films were analyzed as-prepared and after being sputtered for 15 sec with low-energy (200 eV) Ar^+ ions to remove surface contaminants and reveal the bulk composition of the reference peptide films. Spatially-uniform charge neutralization across these samples was provided by beams of low-energy (≤10 eV) electrons and Ar^+ ions. We acquired high-resolution spectra of the Au 4f, C 1s, N 1s, O 1s, and S 2p regions to determine the elemental and chemical composition of the thick peptide films.

For surface adsorption experiments, clean substrates were placed in pure buffer solution in glass vials, the appropriate amount of peptide stock solution then was added to produce an incubation solution of 1.0 mM for pentapeptides and 0.5 mM for decapeptides, corresponding to approximately constant mass concentration. We incubated the substrates at room temperature for 24 h to allow the surface-adsorbed peptides to approach a quasi-equilibrium density. After the incubation period, we filled the incubation well to overflowing with DI water—in effect, infinitely diluting the peptide solutions to prevent the adhesion of any molecules that may have built up at the air-water interface as the substrates pass through that interface. The substrates were rinsed again with DI water after removal from the incubation well and dried under a stream of nitrogen. We collected normal-emission survey and high-resolution spectra for the applicable substrate peaks (Au 4f, Si 2p, Ca 2p, and F 1s) and the peaks corresponding to elements present in the peptides (C 1s, N 1s, and O 1s).

The microfocused X-ray source illuminated a spot of ca. 400×600 μm^2 on the sample; at least three separate spots were analyzed for each sample. Survey spectra were acquired with 1 eV step size at ca. 1.7 eV resolution; high-resolution spectra were acquired with 0.15 eV step size at ca. 0.5 eV resolution. The energy of the monochromated Al Kα X-ray source was regularly calibrated and maintained at 1486.6 ± 0.2 eV. The binding energy (BE) scale of the spectrometer was regularly calibrated based on an automated procedure to produce the Au $4f_{7/2}$, Cu $2p_{3/2}$, and Ag $3d_{5/2}$ peaks within <0.05 eV from the standard reference BE values [38]. The aliphatic C 1s peak was observed at BE = 284.5 ± 0.2 eV for peptide samples. Peak fitting for high-resolution spectra was performed in Unifit (Version 2011), using a convolution of Lorentzian and Gaussian line shapes to fit the individual components [39]. The standard "atomic %" elemental compositions were quantified using calibrated analyzer transmission functions, Scofield sensitivity factors [40], and effective attenuation lengths (EALs) that were calculated using the standard TPP-2M formalism for photoelectrons [36,41].

Statistical analysis

We report all calculated values in terms of their mean plus or minus 95% confidence interval (C.I.) for $n \geq 3$. We used Student's unpaired t-test ($p \leq 0.05$) to determine if mean values were statistically different between datasets.

Percent differences reported in comparative concentration analyses were calculated by normalizing the absolute value of the difference between two concentration measurements by the average of those concentrations. This choice of difference normalization is appropriate for widely divergent pairs of values: presumptively selecting one of the concentration measurements as being the more accurate of the two can systematically bias the comparison.

Results and discussion

The main objective of this study was to develop and validate a combination of preparation protocols and analytical methods for performing reliable, systematic, and quantitative measurements of surface adsorption for a series of model peptides. The work involved three major components: characterization of peptide solutions prepared for deposition experiments, investigation of sample contamination sources, and detailed XPS analysis of peptides adsorbed on inorganic substrates.

Characterization of peptide deposition solutions

Reliable quantitative measurements of peptide adsorption must begin with validated protocols for preparation and characterization of the deposition solutions. Solution concentration is a key parameter in surface adsorption experiments as it can affect the adsorption kinetics, surface saturation, and conformation of adsorbed peptides. The most common method of calculating the concentration of peptides or proteins is based on the dry weight of lyophilized samples. For our repetitive short sequences, the degree of uncertainty produced by the potential presence of associated water or solvent molecules in lyophilized powders was not clear *a priori*, therefore, we performed a comparative analysis of three common methods for measuring the concentration of peptides in solution. Complementary CD measurements substantiated the interpretation of concentration measurements and confirmed the desirable absence of strong

secondary structure or aggregation tendencies for GG–X–GG peptides in deposition solutions.

BCA assay

We found that the BCA protein assay was *ineffective* in determining the concentration of many of the model oligopeptides in our study (Table 1). GG–X–GG peptides (with the notable exceptions of GGPGG and GGSGG) furnished the best results, whereby the BCA-determined concentrations differed by 3–30% from the nominal concentrations based on dry weight. We note that excess weight of powders in this range can be rationalized because the lyophilized peptides can contain physically adsorbed volatiles such as water and trifluoroacetic acid (TFA) introduced during their processing; the effect of such uncertainty in solution concentration on peptide adsorption is discussed in one of the following sections.

BCA and PPII structure

The notable inability of the BCA assay to assess the concentration of the homogenous penta- and decapeptides, X_5 and X_{10}, (Table 1) warranted further investigation. In particular, P_5, which forms a PPII helix, was virtually undetected by the BCA assay; coupled with the better quantification of the unstructured GG–X–GG peptides, this result suggests a possible interference from peptide secondary structure in general or specifically from the PPII structure.

To obtain a colorimetric response in the BCA assay, Cu^{2+} ions must be chelated by the amide backbone of the peptide chain and subsequently reduced [17-19]. Interactions of the Cu^{2+} ions with PPII helices, however, can make this process more complicated. For example, Ma and Wang reported a specific targeting of Cu^{2+} towards PPII structures and, under neutral solution conditions, Cu^{2+} chelation by a PEVK peptide sequence without any evidence of subsequent reduction [42]. We hypothesize, therefore, that PPII structure is responsible for the failure of the BCA assay with P_5. As we expected [43,44], CD measurements (Figure 1) revealed a higher propensity for the formation of PPII helices in most of the X_5 and X_{10} peptides than in their GG–X–GG counterparts. As with P_5, the concentrations of peptides that produced PPII-helix CD signatures were vastly underestimated by the BCA assay. In contrast, the BCA assays yielded reasonable responses with G_5 and G_{10} peptides that did not adopt any secondary structure.

The specific role of the PPII rather than that of any secondary structure was revealed from comparison of S_5 and S_{10} peptides; concentration of S_5 was grossly underestimated by BCA, whereas there was only a 5% difference between the BCA and dry-weight concentrations for S_{10}. We observed that the CD spectrum of S_{10} was characteristic of a β sheet, with a maximum at 195 nm and a single minimum at 221 nm, close to the values of 197 and 222 nm, respectively, reported by Urry *et al.* for poly-L-serine in water [45]. This observation indicates that, as the length of the homo-oligoserine increases from S_5 to S_{10}, the peptide begins to behave like poly-L-serine, which has been shown to form antiparallel

Table 1 Percent differences between peptide concentrations determined by BCA assay and their nominal concentrations based on dry weight[a]

Amino acid	GG–X–GG	X_5	X_{10}
	% Diff. WC[b]	% Diff. WC[b]	% Diff. WC[b]
Glycine (G)	–	17 ± 2	28 ± 9
Alanine (A)	20 ± 2	94 ± 34	–
Aspartic Acid (D)	20 ± 5	157 ± 36	169 ± 24
Glutamic Acid (E)	6 ± 3	128 ± 22	178 ± 5
Lysine (K)	13 ± 6	87 ± 26	101 ± 31
Proline (P)	167 ± 34	193 ± 6	–
Arginine (R)	21 ± 9	105 ± 43	111 ± 41
Serine (S)	26 ± 16	66 ± 25	5 ± 5

[a]Percent difference defined as absolute difference between BCA- and weight-derived concentrations divided by the mean of the two methods.
[b]Percent difference values reported as mean ± 95% C.I., $n = 3$.

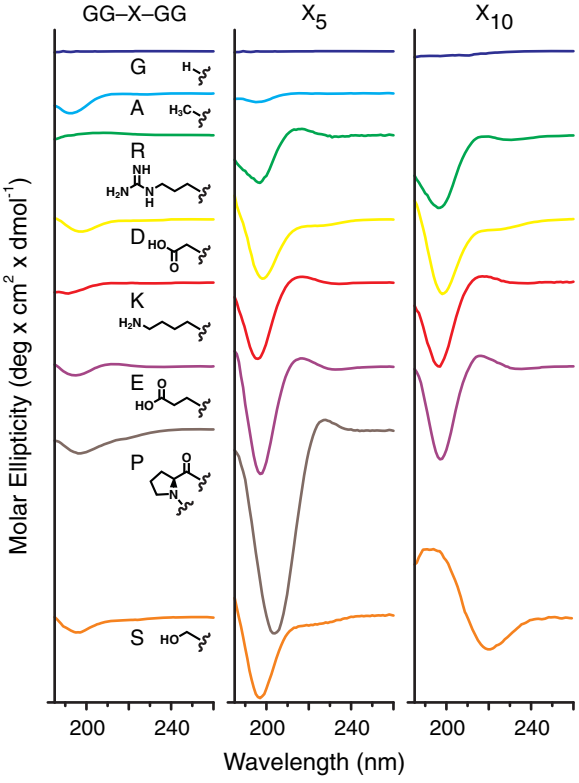

Figure 1 Solution CD spectra of model GG–X–GG and X_n oligopeptides. Spectra were collected in a 1.0-mm path quartz cuvette held at 20°C for ca. 0.2 mM peptide concentrations in 10 mM sodium phosphate buffer (pH 7).

β sheets in aqueous solution [46]. These results suggest that PPII helices in particular, rather than all structured conformations, pose a problem for the BCA assay.

Intrinsic chromophores

Table 2 shows the results of the comparative concentration analysis of model peptides containing an intrinsic chromophore. We used tyrosine or tryptophan as chromophores and omitted cysteine, which has an order of magnitude lower extinction coefficient [21]. Phenylalanine also exhibits strong UV absorbance around 260 nm, but GGFGG showed poor solubility in aqueous solutions and, thus, was unsuitable for comparative analysis. The concentrations of GGWGG and GGYGG in solution, as determined by UV spectroscopy, were lower by ca. 12–16% than their nominal concentrations by weight, which we attribute to the presence of water and/or TFA in the lyophilized powders. We found that the concentration of GGYGG yielded by AA analysis was in good agreement with the result from UV spectroscopy—1.31 and 1.36 mM, respectively. Due to the excellent correlation between the UV spectroscopy and AA analysis of GGYGG, we further investigated the use of tyrosine in our model peptides as a chromophore for peptide quantification.

We examined GG–X–GGY and X_5Y (X = G, A, or P) model peptides that included a C-terminal tyrosine residue as a chromophore. Although G_5 and A_5 were soluble at 1.0 mM concentration in the aqueous stock solutions, G_5Y and A_5Y precipitated out of solution already at a much lower concentration (0.1 mM). Aggregation caused by the appended tyrosine may explain these observations, as Measley *et al.* reported that the addition of a C-terminal tyrosine promotes self-aggregation in alanine-based octamers [47]. Similarly, we observed that GGYGG was water-soluble but GGGGGY formed aggregates, suggesting that the location of the tyrosine residue rather than its mere presence is responsible for the aggregation of peptides labeled with a C-terminal tyrosine.

For GGAGGY and GGPGGY, we found a strong correlation between the concentrations measured by weight, UV absorbance, and AA analysis, with values that were less than 10% different from one another (Table 2). However, we found larger discrepancies in the concentrations of PPPPPY measured by different techniques, particularly for UV spectroscopy versus AA analysis. With the exclusion of proline-based peptides, all concentrations determined by UV spectroscopy and AA analysis were either statistically equal to or less than the nominal weight-based concentration.

Tyrosine chromophore and local structure

We hypothesize that the apparent overestimation of the concentrations of GGPGGY and PPPPPY by UV spectroscopy could be due to secondary structure in these peptides because the extinction coefficient of tyrosine depends heavily upon its local environment [48]. We performed CD spectroscopy on the tyrosine-containing peptide sequences in Table 2 that were water-soluble, with and without their C-terminal tyrosine (Figure 2). The CD spectra of GGAGG, GGPGG, and PPPPP exhibit the characteristic peaks associated with PPII helices, with the structure of the peptide increasing as the amount of proline residues increases [43,49,50]. However, CD analysis of the tyrosine-containing sequences can become complicated if the contributions from aromatic side chains obscure the contribution from the peptide backbone [16,51]. Spectra of the two GG–X–GGY sequences are completely dominated by the contributions from tyrosine, as can be seen by their comparison to the spectrum of GGYGG (Figure 2). We observed a 33% reduction in the molar ellipticity minimum, as well as a shift from 204 to 206 nm, by the addition of a C-terminal tyrosine to P_5. This observation suggests that tyrosine induces structural changes, as the loss in ellipticity far exceeds the linear combination of P_5 and GGYGG. This observation is consistent with our hypothesis that

Table 2 Comparison of different methods for measuring the solution concentration in 10 mM sodium phosphate buffer (pH 7) of peptides containing chromophoric residues

Peptide	Weighed conc.		UV abs. (280 nm)		AA Analysis (mean ± 95% C.I., $n = 3$)		
	(mg/mL)	(mM)	(mM)	% Diff. WC[a]	(mM)	% Diff. WC[a]	% Diff. UV[b]
GGFGG	Low Solubility		–	–	–	–	–
GGWGG	0.41	0.86	0.73	16	–	–	–
GGYGG	0.69	1.53	1.36	12	1.31 ± 0.07	16 ± 6	4 ± 3
GGGGGY	Low Solubility		–	–	–	–	–
GGAGGY	0.55	1.05	0.98	7	0.96 ± 0.04	9 ± 4	2 ± 1
A_5Y	Low Solubility		–	–	–	–	–
GGPGGY	0.56	1.01	1.11	9	1.04 ± 0.04	2 ± 3	7 ± 3
P_5Y	0.80	1.13	1.27	12	0.97 ± 0.11	15 ± 10	27 ± 9

[a]W.r.t. the concentration determined by weight.
[b]W.r.t. the concentration determined by UV absorbance.

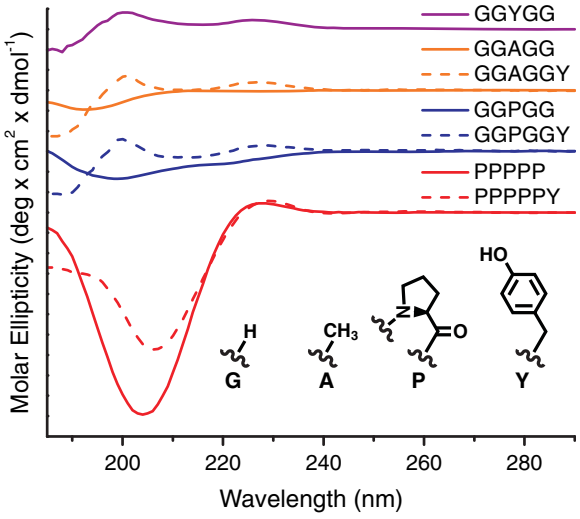

Figure 2 Solution CD spectra of GGYGG and other model peptides with and without a C-terminal tyrosine. Peptide solutions were prepared in a 10 mM sodium phosphate buffer (pH 7) at a peptide concentration of ca. 0.2 mM. All spectra were collected in a 1.0-mm path quartz cuvette held at 20°C. The dashed lines indicate the change in secondary structure when a C-terminal tyrosine was added to the sequence.

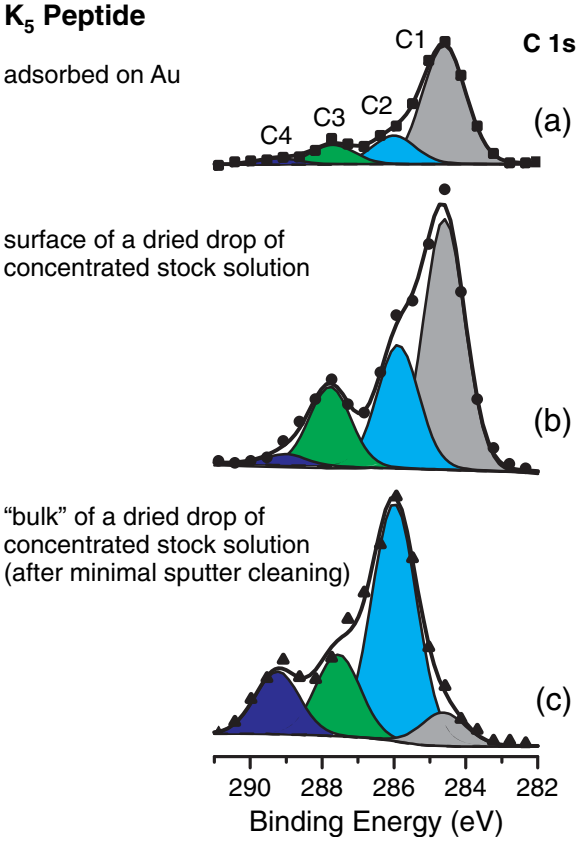

Figure 3 XPS C 1s spectra of K_5 deposited on Au substrates under different conditions. (a) 24 hour incubation at room temperature in a 1 mM peptide solution, 10 mM sodium phosphate buffer (pH 7). **(b)** 3 μL drop of stock solution dried on the substrate. **(c)** Same dried drop as in **(b)** after 15 s of low-energy (200 eV) Ar^+ beam sputtering.

the local environment around tyrosine may be different in the various sequences, resulting in the inaccurate quantification of peptide concentration via C-terminal tyrosine in some of our model peptides.

Effects of surface contamination

Uncontrolled contamination can easily invalidate surface adsorption experiments. Therefore, we looked for evidence of contaminants (*e.g.*, post-synthetic fragments) present in the stock solutions of peptides or competing with peptides during the adsorption experiments. We also investigated the effects produced by post-deposition adventitious contamination on the XPS signatures of surface-adsorbed peptides, as such post-deposition contamination may compromise the interpretation of the XPS data, even if the underlying adsorption experiments were not affected.

Characteristic C 1s components

We incubated Au substrates in a K_5 peptide solution (1.0 mM) and examined the resulting sample by XPS to determine whether the amount of irreversibly-adsorbed peptide was sufficient to distinguish components corresponding to the chemical states of carbon expected in the peptide. Figure 3a shows the high-resolution C 1s region of the XPS spectrum of an Au substrate after incubating for 24 hours in an aqueous 1.0 mM solution of K_5. While we observed four distinct peaks in the C 1s region, the C1 component (BE = 284.5 eV), which corresponds to aliphatic carbon [52-54], dominated the spectrum of the adsorbed peptide layer. Lysine indeed contains aliphatic carbon (methylene groups in its side chain); however, we observed an atomic ratio of 5.1 ± 0.1 for C/N present on the surface, which is in excess of the theoretical C/N ratio of 2.9. This observation indicates the presence of a hydrocarbon contaminant on the surface.

To investigate whether the aliphatic carbon contamination came from the peptide solution or from adventitious carbon in the atmosphere, we formed a thick peptide film on an Au substrate by drying a drop of the K_5 stock solution. The components of the carbon region that correspond to C–O or C–N groups (C2, BE = 285.8 eV), C=O groups (C3, BE = 287.5 eV), and O–C=O or N–C=O groups (C4, BE = 289.1 eV)—that is, carbon species arising from the deposited peptide—are clearly evident in the spectrum of the dried drop (Figure 3b) [53-56]. Although the characteristic peptide peaks in the C 1s region were more prominent than in the adsorbed K_5 layer (Figure 3a), the C/N ratio of the film was 4.0 ± 0.2—that is, above the theoretical value (based on the elemental

composition of K_5 peptide), but 20% lower than for the adsorbed of K_5 layer. The decrease in C/N ratio for a thick film of the dried peptide solution suggests that the observed contamination originates at the surface rather than in the stock solution.

To confirm this inference, we removed the uppermost ca. 0.5 nm of the thick peptide film by sputtering with a low-energy Ar^+ beam [56], and re-analyzed the same spots. The C/N ratio was further reduced to 3.5 ± 0.1 and the C1 component was no longer the predominant component in the spectrum (Figure 3c). The elevated ratio, with respect to the theoretical value, indicates that some non-aliphatic contaminants may remain. However, this analysis of the peptide film supports our inference that the contaminants adsorb primarily from atmosphere. The low energy (200 eV) and short duration (15 sec) of the Ar^+ sputtering would have minimized the damage to the chemistry of the peptide film [56], although details such as the ratio of C2 and C3 components may have been affected, so the spectral envelope in Figure 3c may not be fully characteristic of "bulk" K_5 peptide. The potential sputtering damage, however, would not have affected the inference about removing an adventitious carbon overlayer, because the typical expected Ar^+ damage would have *increased* the C1 component at the expense of the higher-BE components. Finally, we note that this approach works well for freshly prepared samples, but becomes much less effective for samples that have been stored for several days, suggesting that some intermixing of the contaminants into the dried peptide film occurs over time.

Quantifying adventitious contamination

To observe the rate of adsorption of atmospheric carbon-containing species, we exposed a carbon-free Au surface to ambient air for varying times. A blank-buffer control that had been incubated in a phosphate buffer for 24 hours was also analyzed to determine the chemical states of carbon deposited during sample handling (Figure 4). Significant levels of the C1–C4 components were detected; oxygen was also present (Table 3). After the initial measurement, this control sample was Ar^+ sputtered under UHV for 30 sec to yield a clean Au surface; the sample was then exposed to atmosphere in the introduction lock of the XPS instrument. After exposure to ambient air for 1 sec, the carbon levels were 52% of the blank-buffer control levels and the C 1s spectrum contained the C1 and C2 components (Figure 4). We also exposed a sputter-cleaned Au substrate to ambient air for 3 min, as an example of the minimal amount of time a substrate would be exposed to air during sample preparation. We found no statistical difference in the amount of carbon present on the surface after 3 min of exposure as compared to the blank-buffer control, although there was no C3 component after 3 min of exposure (Figure 4). Also,

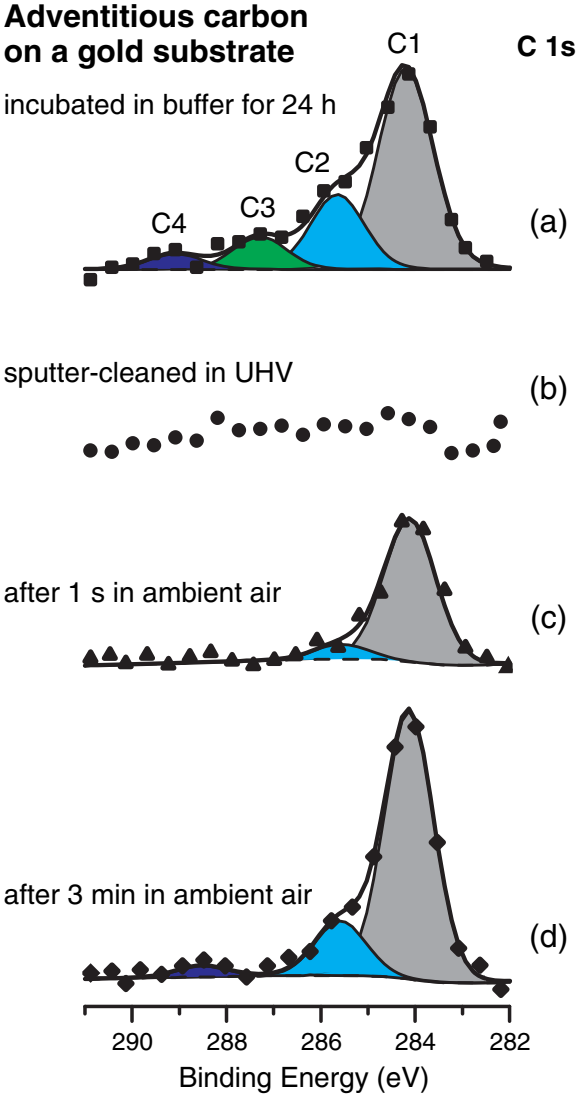

Figure 4 XPS data for the C 1s region of the control samples in surface contamination experiments. (a) Au substrate that was incubated in a blank phosphate buffer for 24 h. Surface contaminants were completely removed by ion beam sputtering and the spot was re-analyzed **(b)**. The sample stage was then exposed to the atmosphere for 1 s **(c)** or 3 min **(d)**, in addition to the time spent purging the loading dock and pumping down for analysis. The spot was sputter-cleaned in UHV prior to each exposure in **(c)** and **(d)**.

Table 3 Atomic percentages of elements on surface contamination control samples[a]

	Au	C	O
Control	60.0 ± 2.3	29.7 ± 2.9	10.3 ± 0.8
Sputtered in UHV	100.0	–	–
Ambient (1 s)	84.7 ± 2.6	15.3 ± 3.1	–
Ambient (3 min)	68.3 ± 2.1	27.1 ± 2.5	4.7 ± 1.0

[a]Values reported as mean ± 95% C.I., $n = 3$.

the blank-buffer control exhibited approximately twice as much oxygen signal, which is most likely due to the increased presence of physisorbed water on its surface. The rapid recovery of the contaminants after sputtering in UHV strongly suggests that, because the carbon contaminants adsorb from the atmosphere, avoiding contamination completely is impractical under typical laboratory conditions. Thus, we minimized the exposure of the substrates to air between cleaning and peptide adsorption to present the peptides to the cleanest surfaces possible, while developing protocols that can be readily reproduced in different laboratories.

Quantification of adsorbed peptides

Figure 5 shows the XPS spectra of a series of model lysine-based peptides, GGKGG, K_5, and K_{10} that were adsorbed onto Au substrates to examine the effects of lysine content and peptide length on irreversible adsorption. The peptide concentrations of the incubation solutions were 1.0 mM and 0.5 mM for penta- and decapeptides, respectively, to ensure roughly the same mass concentrations for the two cases. The substrates were cleaned as before and exposed only briefly to air, while still wet from the final aqueous rinse; nevertheless, the C1 component was the most prominent peak in all of the spectra, indicating the presence of adventitious carbon species. However, the characteristic peptide components, C2–C4, are clearly distinguishable in the spectra of each of the adsorbed peptide layers.

In the N 1s spectra, the main component (N1) is centered at BE = 400.1 eV, corresponding to the amide groups in the peptide backbones and amine groups on the side chains [55,57-59]. The shift to a lower binding energy of the small component (N2; BE ≈ 398.8 eV) is consistent with amide groups that are strongly interacting with inorganic substrates [57,60]. K_5 and K_{10} also exhibited a peak (N3) at BE ≈ 402 eV indicating the presence of protonated amine groups [57-59,61], whereas the single amine group in GGKGG appears to be uncharged after surface adsorption. As there was no adventitious nitrogen detected on the surface of the blank-buffer control, the atomic percentage of nitrogen was used to quantify the surface densities of adsorbed peptides.

Molecular surface densities

We estimated the relative surface densities of the peptides (Table 4) by normalizing the N/Au ratios according to the following equation:

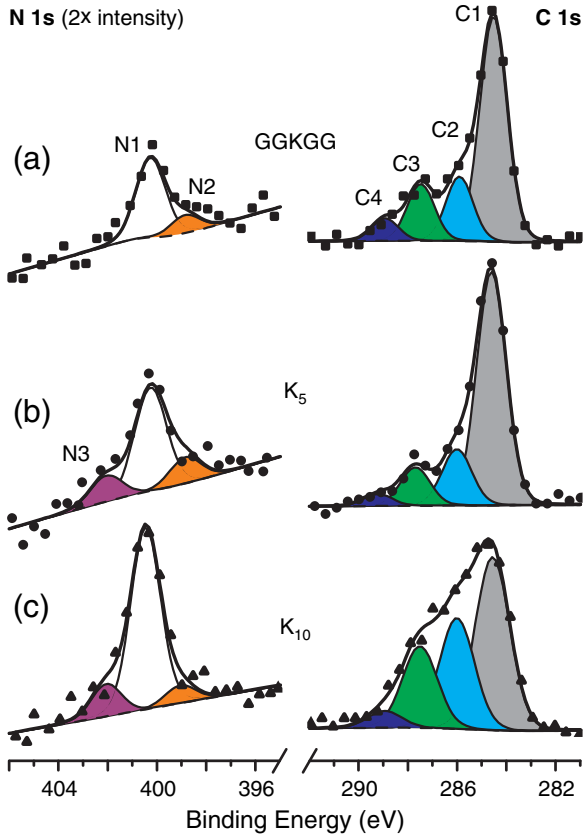

Figure 5 Characteristic XPS signatures of model GGKGG, K_5, and K_{10} peptides deposited on Au substrates. Elemental spectra and fits are shown in the N 1s (at 2× intensity for clarity) and C 1s regions for GGKGG **(a)**, K_5 **(b)**, and K_{10} **(c)**. Substrates were incubated for 24 h in 1.0 mM (GGKGG and K_5) or 0.5 mM (K_{10}) peptide solutions in 10 mM sodium phosphate buffer (pH 7) at room temperature.

This N/Au normalization (where "# of N atoms" and "# of residues" are the numbers of N atoms and residues, respectively, in each peptide) produces an estimate of the surface density of peptide residues. The "atomic %" values used in Eq. (3) are normalized to account for the differences in analyzer transmission function, Scofield sensitivity factors, and EALs between the Au 4f and N 1s photoelectrons. The respective EAL values have not been calculated assuming a specific overlayer structure model; however, they provide an approximate correction for the energy-dependent difference of the sampling depths between Au 4f and N 1s photoelectrons.

$$\text{Norm. N/Au} = (\text{at. \% N/at. \% Au})/(\#\text{ of N atoms}/\#\text{ of residues}) \quad (3)$$

Table 4 Elemental ratios of lysine peptides adsorbed on Au[a]

	Norm. N/Au ratio	Theoretical[b]	Measured	Theoretical[b]	Measured
		C/N	C/N	O/N	O/N
GGKGG	0.051 ± 0.005	2.3	9.1 ± 0.5	0.86	3.6 ± 0.07
K_5	0.041 ± 0.004	2.9	7.6 ± 0.9	0.55	1.7 ± 0.3
K_{10}	0.067 ± 0.003	3.0	5.2 ± 0.4	0.52	1.5 ± 0.2

[a]Values reported as mean ± 95% C.I., $n = 3$.
[b]N-termini are acetylated and C-termini are amidated.

We found a small but statistically significant decrease in the surface density from GGKGG to K_5 and a larger increase of surface density from K_5 to K_{10} (Figure 6, Table 4). A tentative interpretation of this trend in irreversible adsorption indicates a possible competition between electrostatic repulsion (both inter- and intra-molecular) and intra-molecular cooperative adsorption of the lysine residues.

The peptide-specific spectral components in Figure 5 reflect the quantitative results in Figure 6 and Table 4. The K_{10} spectra clearly show the highest intensity of N 1s and peptide-specific C2–C4 components. The C2–C4 components are slightly decreased from GGKGG to K_5, reflecting the lower peptide coverage. The N 1s components are noticeably stronger for K_5 than for GGKGG, corresponding to nearly double the number of N atoms in each molecule of the former.

Sample stoichiometry

Quantifying the sample stoichiometry is complicated by the presence of coadsorbates, which is most clearly revealed by the elevated C/N and O/N ratios (Table 4). While the excess oxygen is likely from physically adsorbed water molecules, the excess carbon clearly indicates that, despite our efforts to limit the exposure of the surfaces to air, carbonaceous coadsorbates or contaminants are still present.

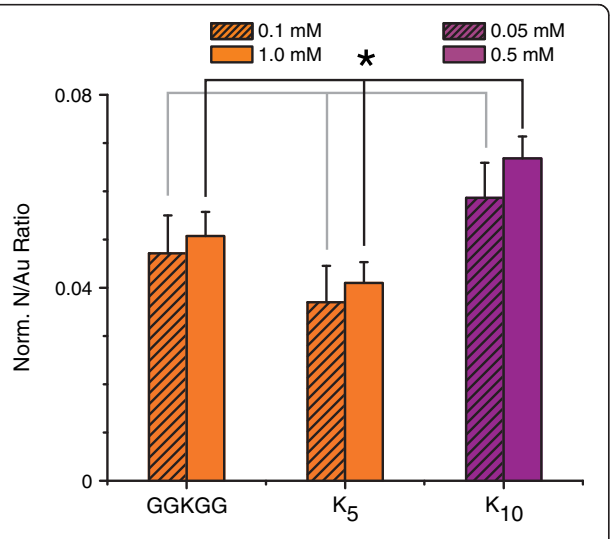

Figure 6 Normalized N/Au ratios for GGKGG, K_5, and K_{10} peptides adsorbed on Au from solutions of different concentrations. For each peptide, a 10-fold dilution in 10 mM sodium phosphate buffer (pH 7) was tested for differences after adsorption for 24 h at room temperature. N/Au ratios are normalized by the average number of nitrogen atoms per residue for each peptide. (*) Denotes significant difference ($p < 0.05$) between a pair of values.

To assess at which stage—before or after peptide adsorption—they adhere to the surface, we repeated the experiments with substrates that had been intentionally fouled with aliphatic molecules after cleaning. In the "hexane rinse" experiments of Figure 7, the clean Au substrates where blown dry with nitrogen gas, rinsed with hexanes, and then blown dry again before placing them in the incubation wells filled with a phosphate buffer. The surface densities of peptides deposited after the hexanes rinse trend towards higher values as the number of lysine residues increases (Figure 7, top). We observed, however, that on the substrates rinsed with hexanes the atomic % of Au dramatically decreased (Figure 7, bottom) as the amount of surface-adsorbed peptide increased. This attenuation of the Au peak indicates that the total amount of material adsorbed on the surface is increasing on the hexanes-rinsed substrates after the adsorption of K_5 and K_{10}, suggesting that the peptides are adsorbing on top of rather than displacing the surface-adsorbed hydrocarbon layer.

In contrast, the atomic % of Au remained fairly constant when the peptides were adsorbed to clean Au substrates (Figure 7, bottom), despite the surface density of peptide residues being much higher for K_{10} than for GGKGG or K_5. This observation suggests that in our standard experiments the peptides do not adsorb onto a layer of surface contaminants. Instead, the peptides appear to either displace surface contaminants that are present *before* peptide adsorption, or, alternatively, the peptides leave unoccupied surface sites where the contaminants adsorb *after* peptide adsorption, when the samples are exposed to air; the trend in intensity of the C1 component in Figure 5 could be rationalized in terms of either interpretation. We believe that the contamination analysis shows that despite the detected coadsorbates or contaminants, their presence minimally influences peptide adsorption quantified in our experiments, and thus our protocols are suitable for evaluating the differential irreversible adsorption of model peptides on Au surfaces.

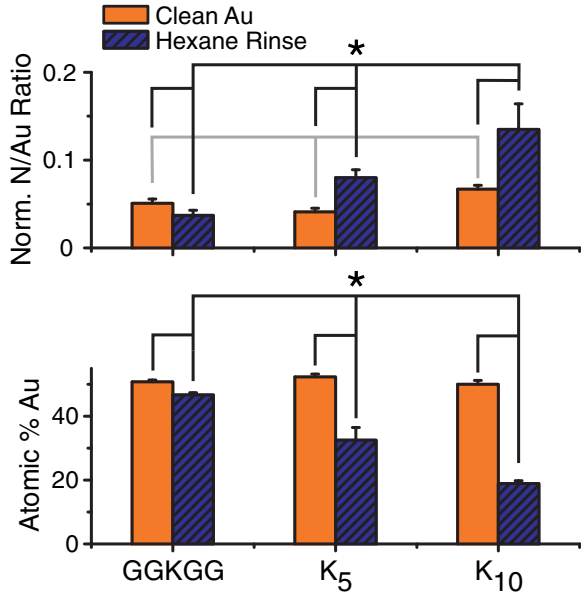

Figure 7 Effects of aliphatic surface contamination on adsorption of peptides. N/Au ratios (top) and atomic % of Au (bottom) are compared for samples deposited on gold substrates immediately after cleaning (orange) and after a rinse in hexanes (blue). Both types of substrates were incubated in 1.0 mM (GGKGG and K_5) or 0.5 mM (K_{10}) peptide solutions in 10 mM sodium phosphate buffer (pH 7) at room temperature. N/Au ratios are normalized by the average number of nitrogen atoms per residue for each peptide. (*) Denotes significant difference ($p < 0.05$) between a pair of values.

Photoelectron attenuation

The minimal variation of the apparent attenuation of the gold substrate XPS signal (orange bars in Figure 7, bottom) among the peptide samples deposited using our standard protocol indicates that the photoelectron attenuation is produced by a combination of the peptide and adventitious adsorbates. While the relative amounts of these two overlayer components change as the function of the amount of adsorbed peptides, the total effective overlayer thickness is similar in all cases. Accordingly, the simple normalized N/Au at. % ratios of Eq. (3) should provide a reliable quantitative measure of the variation in the amount of the adsorbed peptides (because the Au signal provides an approximately constant internal reference). Conversely, developing and validating a rigorous model that accounts for the signal attenuation across a wide range of adsorbed peptide samples would be very challenging, as such a model would need to include information about the overlayer structure, *e.g.*, the relative distribution of the peptide and adventitious components in each case.

Effect of peptide concentration

To test whether uncertainty in the nominal concentration of the peptide solution (as determined from the weight of dry powder) significantly affects the observed surface densities of the adsorbed peptides, we incubated clean substrates in peptide solutions diluted tenfold (0.1 mM or 0.05 mM) with respect to the standard deposition solutions used in the experiments described above. We observed no statistical difference in the surface density *between* the series of peptides adsorbed at the standard or diluted concentration (Figure 6). As we previously discussed, the nominal concentration by weight is within 30% of the reliable solution concentration values determined by different methods; thus, we believe that the nominal solution concentration based on the dry weight of peptide is sufficiently accurate for our experiments. While we observed no difference in surface densities over a tenfold concentration range in the case of the lysine peptides, we note that other peptide systems could be more sensitive to the incubation concentration with respect to surface adsorption.

Peptide adsorption on different substrates

We find that the XPS data in the N 1s and C 1s regions were similar for K_{10} adsorbed on different inorganic substrates (Figure 8). Hydrocarbon contaminants were present on the surface of hydrophilic substrates, such as fused quartz, although at lower levels than on the Au substrates. The N 1s spectra of K_{10} had three components on all surfaces except on fused quartz, where the spectrum exhibited a weak peak in the region that corresponds to protonated amines and no peak related to surface-interacting amide/amine groups. This observation suggests that protonated amines on the lysine side chains might preferentially form ion pairs with negatively charged silicic acid groups on the quartz surface. The raw atomic percentages of nitrogen were not directly comparable across the different substrates because they depend on the other elements present, so small deviations (due to BE, normalization, and fitting) in the substrate and adventitious carbon signals—always the highest fractions present—can translate to large relative deviations in the nitrogen signal—typically the lowest fraction present. Therefore, we normalized the nitrogen signal to that of the substrate elements (in at. % normalization, *i.e.*, a generalized form of Eq. [3]) to estimate the relative molecular surface coverages of peptides on a given substrate. This normalization procedure resulted in a lower overall uncertainty for comparing the surface densities of peptides than the uncertainty of directly comparing the raw nitrogen at. % values. The highest surface density of K_{10} was observed on gold substrates, while the lowest K_{10} densities were observed on fused silica and Si wafer substrates.

Conclusions

We evaluated methods for quantifying model oligopeptides both in solution and after their adsorption onto inorganic substrates.

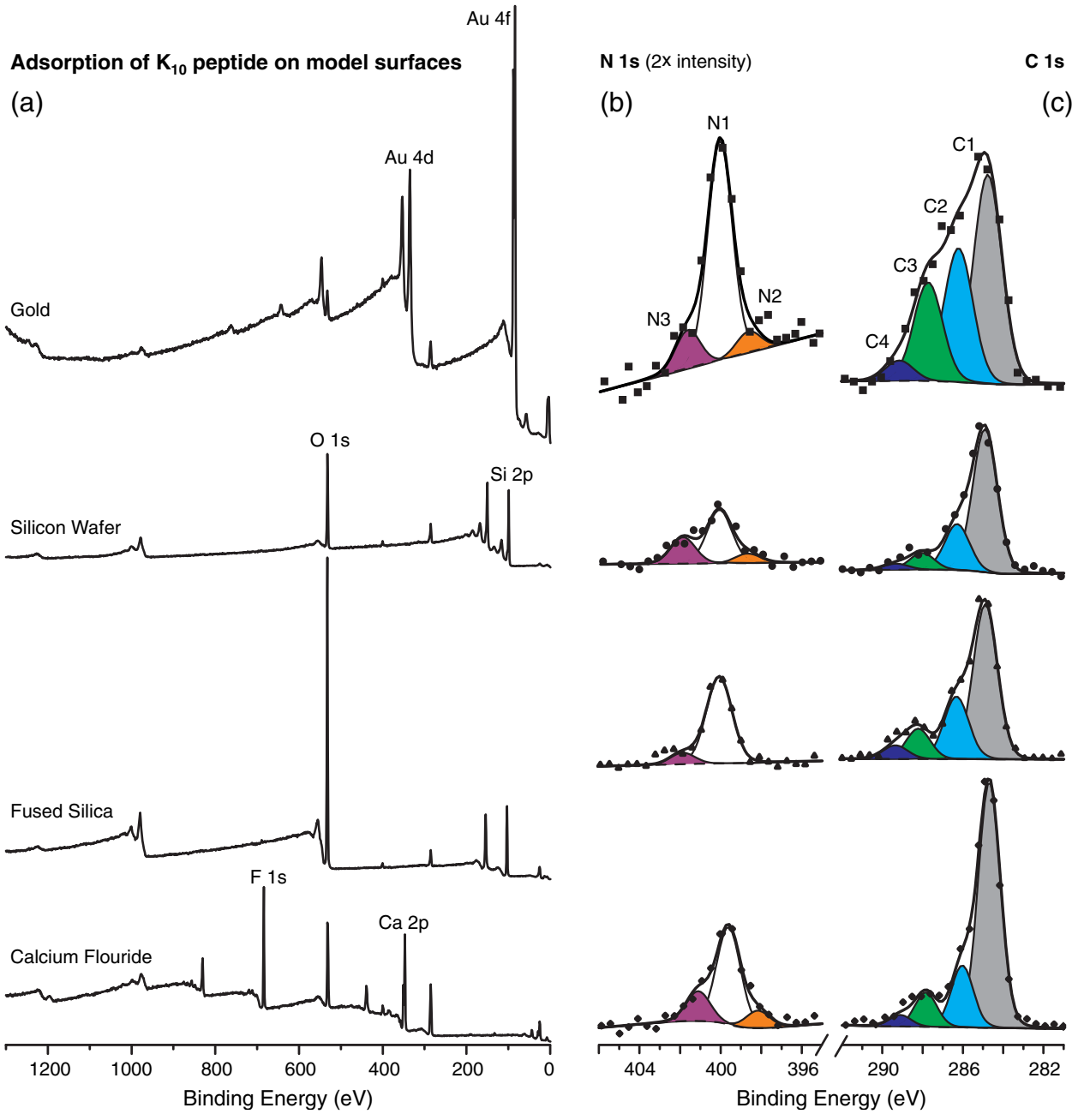

Figure 8 Characteristic XPS surveys and elemental spectra of K_{10} deposited on different inorganic substrates. Clean substrates were incubated for 24 h in a 0.5 mM peptide solution (10 mM sodium phosphate buffer, pH 7) at room temperature. Surveys **(a)**, and elemental spectra of the N 1s **(b)** and C 1s **(c)** regions are shown as raw XPS intensities.

Each of the three methods that we investigated to determine peptide concentration in solution proved to have shortcomings. We found good agreement between UV spectroscopy and AA analysis, but the addition of a C-terminal tyrosine for UV measurements resulted in solubility problems and structural changes for many of our small model peptides. The structure of some of the model peptides apparently affected the BCA assay. In general, the nominal concentration based on the weight of as-received lyophilized peptide was within 30% of reliable measurements by the other methods; we hypothesize that the possible presence of water and/or TFA in lyophilized samples is the main source of this uncertainty of weight-based concentration values. In a separate test, we observed no statistically significant differences between the surface densities of our model peptides adsorbed from solutions differing

tenfold in peptide concentration. We therefore conclude that determining peptide concentrations from the dry weight of the dissolved powder is sufficiently accurate for carrying out systematic adsorption experiments with our model peptides. The estimated uncertainty of 30% is also likely to be more generally applicable to the determination of peptide concentrations based on their dry weight; whether this level of uncertainty in peptide concentrations significantly affects surface adsorption should be determined for each specific peptide-surface system.

XPS proved useful for quantifying the amount of the model peptides that were irreversibly adsorbed onto a surface. Hydrocarbon contaminants were present on the peptide-coated substrates, but Ar^+ sputtering showed that the bulk of the contaminants adsorb from the atmosphere rather than from the stock solutions of purified peptides. In contrast to the carbon contamination, we found that the substrates examined do not become contaminated with any nitrogen-containing species. This observation enabled us to calculate the relative surface densities of different peptides on the same surface; however, we refrained from quantitatively comparing the relative surface densities across substrates due to differences in the quantification of the reference substrate peaks. The similarity of the peptide peaks on different surfaces indicates that XPS is a viable method for measuring differential adsorption of peptides on a wide selection of substrates [62].

Finally, we found that not only were surface contaminants present on all substrates, but that the amounts of these contaminants varied. Just a few minutes of exposure to ambient air can produce a significant amount of adventitious contamination; therefore, completely avoiding contamination is likely impractical, if not impossible, in experiments involving peptide adsorption from solutions. Fortunately, we determined that XPS is useful for distinguishing between the adsorbed peptides and carbonaceous contaminants on samples prepared following practical protocols; in contrast, techniques that measure molecular adsorption non-specifically (*e.g.,* SPR and QCM) may prove inadequate in distinguishing between peptide and non-peptide molecules (*e.g.,* contaminants, detergents, or coadsorbates). We stress that a detailed analysis of the characteristic spectral components is necessary to verify specific peptide deposition and to understand potential sources and effects of contamination; relying only on total elemental atomic % values can lead to both false positive and false negative interpretations of the XPS data for low-coverage peptide films.

Competing interests
The authors declare that they have no competing interests.

Authors' contributions
KPF developed and validated experimental protocols, as well as collected and interpreted data. TDC and DYP conceived the study. TDC guided the design of peptide concentration measurements and participated in the interpretation of CD data. DYP helped to design the XPS measurements and to interpret the XPS data. All authors participated in drafting the manuscript and read and approved the final manuscript.

Authors' information
KPF and DYP are AVS members.

Acknowledgments
Support for this work was provided by the Office of Naval Research (ONR) and the Air Force Office of Scientific Research (AFOSR). KPF thanks the National Research Council for a Postdoctoral Fellowship at NRL during the initial stages of this project. The authors also thank Dr. George P. Anderson (NRL) for the use of Jasco J-815 spectrometer. DYP thanks Dr. Robert Willett (Bell Labs) for useful discussions and for peptide samples provided for initial comparative analysis.

Author details
[1]Division of Chemistry, Naval Research Laboratory, Washington, DC 20375-5342, USA. [2]Department of Physics, University of Maryland, College Park, MD 20742, USA. [3]Current address: International Iberian Nanotechnology Laboratory (INL), 4715-330, Braga, Portugal.

Received: 12 June 2013 Accepted: 17 July 2013
Published: 19 August 2013

References
1. Bange A, Halsall HB, Heineman WR (2005) Microfluidic immunosensor systems. Biosens Bioelectron 20(12):2488–2503
2. Vogler EA (2012) Protein adsorption in three dimensions. Biomaterials 33(5):1201–1237
3. Nabika H, Takimoto B, Murakoshi K (2008) Molecular separation in the lipid bilayer medium: electrophoretic and self-spreading approaches. Anal Bioanal Chem 391(7):2497–2506
4. Yebra DM, Kiil S, Dam-Johansen K (2004) Antifouling technology–past, present and future steps towards efficient and environmentally friendly antifouling coatings. Prog Org Coat 50:75–104
5. Garcia AJ (2006) Interfaces to control cell-biomaterial adhesive interactions. Adv Polym Sci 203:171–190
6. Lord MS, Foss M, Besenbacher F (2010) Influence of nanoscale surface topography on protein adsorption and cellular response. Nano Today 5(1):66–78
7. Raut VP, Agashe MA, Stuart SJ, Latour RA (2005) Molecular dynamics simulations of peptide-surface interactions. Langmuir 21(4):1629–1639
8. Heinz H, Farmer BL, Pandey RB, Slocik JM, Patnaik SS, Pachter R, Naik RR (2009) Nature of molecular interactions of peptides with gold, palladium, and Pd-Au bimetal surfaces in aqueous solution. J Am Chem Soc 131 (28):9704–9714
9. Horinek D, Serr A, Geisler M, Pirzer T, Slotta U, Lud SQ, Garrido JA, Scheibel T, Hugel T, Netz RR (2008) Peptide adsorption on a hydrophobic surface results from an interplay of solvation, surface, and intrapeptide forces. Proc Natl Acad Sci USA 105(8):2842–2847
10. Armstrong J, Perham RN, Walker JE (1981) Domain structure of bacteriophage fd adsorption protein. FEBS Lett 135(1):167–172
11. Thyparambil AA, Wei Y, Latour RA (2012) Determination of peptide-surface adsorption free energy for material surfaces not conducive to SPR or QCM using AFM. Langmuir 28(13):5687–5694
12. Wei Y, Latour RA (2008) Determination of the adsorption free energy for peptide-surface interactions by SPR spectroscopy. Langmuir 24(13):6721–6729
13. O'Brien CP, Stuart SJ, Bruce DA, Latour RA (2008) Modeling of peptide adsorption interactions with a poly(lactic acid) surface. Langmuir 24 (24):14115–14124
14. Mermut O, Phillips DC, York RL, McCrea KR, Ward RS, Somorjai GA (2006) In situ adsorption studies of a 14-amino acid leucine-lysine peptide onto hydrophobic polystyrene and hydrophilic silica surfaces using quartz crystal microbalance, atomic force microscopy, and sum frequency generation vibrational spectroscopy. J Am Chem Soc 128(11):3598–3607
15. Weidner T, Apte JS, Gamble LJ, Castner DG (2010) Probing the orientation and conformation of α-helix and β-strand model peptides on self-assembled monolayers using sum frequency generation and NEXAFS spectroscopy. Langmuir 26(5):3433–3440

16. Chakrabartty A, Kortemme T, Padmanabhan S, Baldwin RL (1993) Aromatic side-chain contribution to far-ultraviolet circular-dichroism of helical peptides and its effect on measurement of helix propensities. Biochemistry 32(21):5560–5565
17. Stoscheck CM (1990) Quantitation of protein. Methods Enzymol 182:50–68
18. Smith PK, Krohn RI, Hermanson GT, Mallia AK, Gartner FH, Provenzano MD, Fujimoto EK, Goeke NM, Olson BJ, Klenk DC (1985) Measurement of protein using bicinchoninic acid. Anal Biochem 150(1):76–85
19. Wiechelman KJ, Braun RD, Fitzpatrick JD (1988) Investigation of bicinchoninic acid protein assay: identification of the groups responsible for color formation. Anal Biochem 175:231–237
20. Lindroth P, Mopper K (1979) High performance liquid chromatographic determination of subpicomole amounts of amino acids by precolumn fluorescence derivatization with o-phthaldialdehyde. Anal Chem 51(11):1667–1674
21. Gill SC, Vonhippel PH (1989) Calculation of protein extinction coefficients from amino-acid sequence data. Anal Biochem 182(2):319–326
22. Mayer MM, Miller JA (1970) Photometric analysis of proteins and peptides at 191-194 mμ. Anal Biochem 36(1):91–100
23. Wei Y, Latour RA (2009) Benchmark experimental data set and assessment of adsorption free energy for peptide-surface interactions. Langmuir 25(10):5637–5646
24. Wei Y, Latour RA (2010) Correlation between desorption force measured by atomic force microscopy and adsorption free energy measured by surface plasmon resonance spectroscopy for peptide-surface interactions. Langmuir 26(24):18852–18861
25. Willett RL, Baldwin KW, West KW, Pfeiffer LN (2005) Differential adhesion of amino acids to inorganic surfaces. Proc Natl Acad Sci USA 102(22):7817–7822
26. Hlady V, Reinecke DR, Andrade JD (1986) Fluorescence of adsorbed protein layers. I. Quantitation of total internal reflection fluorescence. J Colloid Interface Sci 111(2):555–569
27. Wagner MS, Horbett TA, Castner DG (2003) Characterizing multicomponent adsorbed protein films using electron spectroscopy for chemical analysis, time-of-flight secondary ion mass spectrometry, and radiolabeling: capabilities and limitations. Biomaterials 24(11):1897–1908
28. Benesch J, Askendal A, Tengvall P (2000) Quantification of adsorbed human serum albumin at solid interfaces: a comparison between radioimmunoassay (RIA) and simple null ellipsometry. Colloids Surf, B 18(2):71–81
29. Yoshinari M, Kato T, Matsuzaka K, Hayakawa T, Shiba K (2010) Prevention of biofilm formation on titanium surfaces modified with conjugated molecules comprised of antimicrobial and titanium-binding peptides. Biofouling 26(1):103–110
30. Seker UOS, Wilson B, Sahin D, Tamerler C, Sarikaya M (2009) Quantitative affinity of genetically engineered repeating polypeptides to inorganic surfaces. Biomacromolecules 10(2):250–257
31. Mrksich M, Sigal GB, Whitesides GM (1995) Surface plasmon resonance permits in situ measurement of protein adsorption on self-assembled monolayers of alkanethiolates on gold. Langmuir 11(11):4383–4385
32. Fears KP, Latour RA (2009) Assessing the influence of adsorbed-state conformation on the bioactivity of adsorbed enzyme layers. Langmuir 25(24):13926–13933
33. Sivaraman B, Fears KP, Latour RA (2009) Investigation of the effects of surface chemistry and solution concentration on the conformation of adsorbed proteins using an improved circular dichroism method. Langmuir 25(5):3050–3056
34. Paynter RW, Ratner BD, Horbett TA, Thomas HR (1984) XPS studies on the organization of adsorbed protein films on fluoropolymers. J Colloid Interface Sci 101(1):233–245
35. Tidwell CD, Castner DG, Golledge SL, Ratner BD, Meyer K, Hagenhoff B, Benninghoven A (2001) Static time-of-flight secondary ion mass spectrometry and x-ray photoelectron spectroscopy characterization of adsorbed albumin and fibronectin films. Surf Interface Anal 31(8):724–733
36. Jablonski A, Powell CJ (2002) The electron attenuation length revisited. Surf Sci Rep 47(2–3):35–91
37. He L, Navarro AE, Shi Z, Kallenbach NR (2012) End effects influence short model peptide conformation. J Am Chem Soc 134(3):1571–1576
38. Seah MP, Gilmore LS, Beamson G (1998) XPS: Binding energy calibration of electron spectrometers. V. Re-evaluation of the reference energies. Surf Interface Anal 26(9):642–649
39. Hesse R, Streubel P, Szargan R (2007) Product or sum: comparative tests of Voigt, and product or sum of Gaussian and Lorentzian functions in the fitting of synthetic Voigt-based X-ray photoelectron spectra. Surf Interface Anal 39(5):381–391
40. Scofield JH (1976) Hartree-Slater subshell photoionization cross-sections at 1254 and 1487 eV. J Electron Spectrosc Relat Phenom 8 (2):129–137
41. Tanuma S, Powell CJ, Penn DR (1994) Calculations of electron inelastic mean-free paths. V. Data for 14 organic-compounds over the 50-2000 eV range. Surf Interface Anal 21(3):165–176
42. Ma K, Wang KA (2003) Binding of copper(II) ions to the polyproline II helices of PEVK modules of the giant elastic protein titin as revealed by ESI-MS, CD, and NMR. Biopolymers 70(3):297–309
43. Shi Z, Chen K, Liu Z, Ng A, Bracken WC, Kallenbach NR (2005) Polyproline II propensities from GGXGG peptides reveal an anticorrelation with β-sheet scales. Proc Natl Acad Sci USA 102(50):17964–17968
44. Shi Z, Woody RW, Kallenbach NR (2002) Is polyproline II a major backbone conformation in unfolded proteins? Adv Protein Chem 62:163–240
45. Quadrifoglio F, Urry DW (1968) Ultraviolet rotatory properties of polypeptides in solution. II. Poly-L-serine. J Am Chem Soc 90(11):2760–2765
46. Gupta A, Tandon P, Gupta VD, Rastogi S (1997) Vibrational dynamics and heat capacity of β-poly(L-serine). Polymer 38(10):2389–2397
47. Measey TJ, Smith KB, Decatur SM, Zhao LM, Yang GL, Schweitzer-Stenner R (2009) Self-aggregation of a polyalanine octamer promoted by its C-terminal tyrosine and probed by a strongly enhanced vibrational circular dichroism signal. J Am Chem Soc 131(51):18218–18219
48. Mach H, Middaugh CR, Lewis RV (1992) Statistical determination of the average values of the extinction coefficients of tryptophan and tyrosine in native proteins. Anal Biochem 200(1):74–80
49. Ding L, Chen K, Santini PA, Shi Z, Kallenbach NR (2003) The pentapeptide GGAGG has PII conformation. J Am Chem Soc 125(27):8092–8093
50. Darnell G, Orgel JPRO, Pahl R, Meredith SC (2007) Flanking polyproline pequences inhibit β-sheet structure in polyglutamine segments by inducing PPII-like helix structure. J Mol Biol 374(3):688–704
51. Sreerama N, Manning MC, Powers ME, Zhang JX, Goldenberg DP, Woody RW (1999) Tyrosine, phenylalanine, and disulfide contributions to the circular dichroism of proteins: Circular dichroism spectra of wild-type and mutant bovine pancreatic trypsin inhibitor. Biochemistry 38(33):10814–10822
52. Estrade-Szwarckopf H (2004) XPS photoemission in carbonaceous materials: a "defect" peak beside the graphitic asymmetric peak. Carbon 42(8–9):1713–1721
53. Lin Z, Strother T, Cai W, Cao X, Smith LM, Hamers RJ (2002) DNA attachment and hybridization at the silicon (100) surface. Langmuir 18(3):788–796
54. Steffens GCM, Nothdurft L, Buse G, Thissen H, Hocker H, Klee D (2002) High density binding of proteins and peptides to poly(D,L-lactide) grafted with polyacrylic acid. Biomaterials 23(16):3523–3531
55. Iucci G, Battocchio C, Dettin M, Gambaretto R, Di Bello C, Borgatti F, Carravetta V, Monti S, Polzonetti G (2007) Peptides adsorption on TiO_2 and Au: Molecular organization investigated by NEXAFS, XPS and IR. Surf Sci 601(18):3843–3849
56. Lock EH, Petrovykh DY, Mack P, Carney T, White RG, Walton SG, Fernsler RF (2010) Surface composition, chemistry, and structure of polystyrene modified by electron-beam-generated plasma. Langmuir 26(11):8857–8868
57. Petrovykh DY, Kimura-Suda H, Tarlov MJ, Whitman LJ (2004) Quantitative characterization of DNA films by X-ray photoelectron spectroscopy. Langmuir 20(2):429–440
58. Polzonetti G, Battocchio C, Dettin M, Gambaretto R, Di BC, Carravetta V, Monti S, Iucci G (2008) Self-assembling peptides: A combined XPS and NEXAFS investigation on the structure of two dipeptides Ala-Glu, Ala-Lys. Mater Sci Eng C 28(2):309–315
59. Yam C-M, Zheng L, Salmain M, Pradier C-M, Marcus P, Jaouen G (2001) Labelling and binding of poly-(L-lysine) to functionalised gold surfaces. Combined FT-IRRAS and XPS characterisation. Colloids Surf, B 21(4):317–327
60. Jewett S, Zemlyanov D, Ivanisevic A (2011) Adsorption of mixed peptide/thiol adlayers on InAs: Assessment of different functionalization

strategies using X-ray photoelectron spectroscopy. J Phys Chem C 115(29):14244–14252
61. Bassim ND, Dressick WJ, Fears KP, Stroud RM, Clark TD, Petrovykh DY (2012) Layer-by-layer assembly of heterogeneous modular nanocomposites. J Phys Chem C 116(2):1694–1701
62. Fears KP, Petrovykh DY, Photiadis SJ, Clark TD (2013) Circular dichroism analysis of cyclic β-helical peptides adsorbed on planar fused quartz. Langmuir 29(32):10095–10101

doi:10.1186/1559-4106-8-20
Cite this article as: Fears *et al.*: Evaluating protocols and analytical methods for peptide adsorption experiments. *Biointerphases* 2013 **8**:20.